Modified Fresnel Coefficients for Huygens' Sources in FDTD

Torleif Martin, Lars Pettersson
Swedish Defence Research Agency
Dept. of Microwave Technology
P.O. Box 1165
S-581 11 Linköping, SWEDEN

Abstract: *Scattering of electromagnetic fields from objects on or beneath the ground can be analyzed with the Finite-Difference Time-Domain (FDTD) method. The equivalence principle can be utilized for generation of incident plane waves where the Fresnel reflection and refraction coefficients are multiplied by the pulse spectrum in the frequency domain and the result is transformed into the time-domain. Errors will appear in the Huygens' sources due to numerical dispersion where the main errors come from the use of analytical reflection and refraction coefficients. Their influence on the accuracy is generally negligible for applications where the scattered field from the object is greater than the numerical errors introduced. However, if weak scattering events are considered, such as for objects buried in the ground, the dispersion errors can be of the same order of magnitude as the scattered field. In this paper we derive the modified Fresnel coefficients for a homogeneous lossy ground which are consistent with the FDTD algorithm and can be used in the Huygens' sources for suppressing numerical errors. It is shown that the modified Fresnel coefficients reduces the noise level for an empty FDTD volume by 30 to 60 dB. As an application example, the far-zone scattering of a buried dipole is considered.*

1 Introduction

Numerical simulation of electromagnetic scattering from objects on or below ground is an important topic in applications such as ground penetrating radar and synthetic aperture radar. Both time-domain methods and frequency domain methods are represented among recently published work [1–12]. Time-domain methods such as FDTD have the advantage of generating results for the entire frequency range in a single simulation. In scattering applications where the transmitting source is positioned far away from the scatterer, the incident field can be approximated by a plane wave. If the plane wave is created using a Huygens' surface enclosing the object [13], a large computational volume implies large dispersion errors of the incident field. One way to overcome this for free-space simulations, is to use dispersion compensated Huygens' sources [14], applied directly in the time domain.

When a ground is included as a homogeneous lossy half-space, the incident, reflected and refracted fields are preferably pre-calculated in the frequency domain where it is relatively simple to apply the Fresnel reflection and refraction coefficients to the incident pulse spectrum.

However, even if the incident fields are dispersion compensated according to [14], our experience shows that the errors due to the use of analytical Fresnel coefficients are much greater than the dispersion errors occurring when a plane wave propagates across the computational volume. The reason for this is that the analytical Fresnel coefficients are not consistent with FDTD.

Numerical properties of reflection coefficients in FDTD have been studied in several papers. Recently Hirono *et. al.* [15] derived theoretical reflection coefficients for a lossless dielectric-dielectric interface for a 2-D case. In [16] reflection coefficients of a staircased air-dielectric interface are studied for a boundary tilted 45° with respect to the FDTD-lattice. Theoretical expressions for the reflection coefficients at interfaces of perfectly matched layers (PML) have also been presented by Fang *et. al.* [17].

In this paper we derive modified FDTD Fresnel reflection and refraction coefficients for oblique incidence in 3-D for polarizations parallel as well as perpendicular to the plane of incidence. These coefficients are intended for plane wave excitation in scattering applications where the ground is modeled as a homogeneous lossy dielectric half-space. Using these Fresnel coefficients, significant improvements of scattering results for weak scatterers (such as buried objects) are obtained.

The ground model used here is a homogeneous lossy dielectric half-space with the interface aligned with the FDTD-lattice axis. The tangential electric field components in the top-layer are updated using the constitutive

parameters of the ground while the normal components, a half cell size above, are entirely updated in the free-space region. Hence, no adjustment of the interface position is applied using harmonic and arithmetic mean values of the permittivities at the interface such as described in [15].

2 Huygens' sources for plane wave incidence on a homogeneous ground

Plane wave incidence upon a homogeneous half space, using a broad band pulse requires that the incident, reflected and transmitted fields are calculated in the time-domain on a Huygens' surface enclosing the scattering object. This procedure has been described in [1] for stratified media. If the scatterer is large it is normally favorable to use the total-field/scattered-field method using a Huygens' surface.

The principle of implementing the Huygens' sources at an interface between free space and a lossy homogeneous half-space is described briefly as follows. Above the ground, the Fresnel reflection coefficients, $\Gamma_{\parallel}$ and $\Gamma_{\perp}$, are calculated in the frequency domain for a given incidence angle, θ_i, to the surface normal. The incident pulse spectrum is multiplied with the corresponding reflection coefficient and the result is transformed into the time-domain. These time-domain fields are stored in arrays, one for each field component. Given the retarded times for the incident and reflected fields at each point of the Huygens' surface, the fields can be extracted by a table look-up procedure [18],[19]. The situation within the homogeneous ground is treated in a similar way, using the Fresnel refraction coefficients $T_{\parallel}$ and $T_{\perp}$, although a lossy ground requires storage of time-domain field components at each layer in the ground due to the frequency dispersion.

Consider the situation in Fig. 1. The analytical Fresnel coefficients for the electric field perpendicular and parallel to the plane of incidence are given by [20]

$$\Gamma_{\parallel} = \frac{n^2\cos\theta_i - \sqrt{n^2-\sin^2\theta_i}}{n^2\cos\theta_i + \sqrt{n^2-\sin^2\theta_i}} \quad (1)$$

$$\Gamma_{\perp} = \frac{\cos\theta_i - \sqrt{n^2-\sin^2\theta_i}}{\cos\theta_i + \sqrt{n^2-\sin^2\theta_i}}. \quad (2)$$

$$T_{\parallel} = \frac{2n\cos\theta_i}{n^2\cos\theta_i + \sqrt{n^2-\sin^2\theta_i}} \quad (3)$$

$$T_{\perp} = \frac{2\cos\theta_i}{\cos\theta_i + \sqrt{n^2-\sin^2\theta_i}} \quad (4)$$

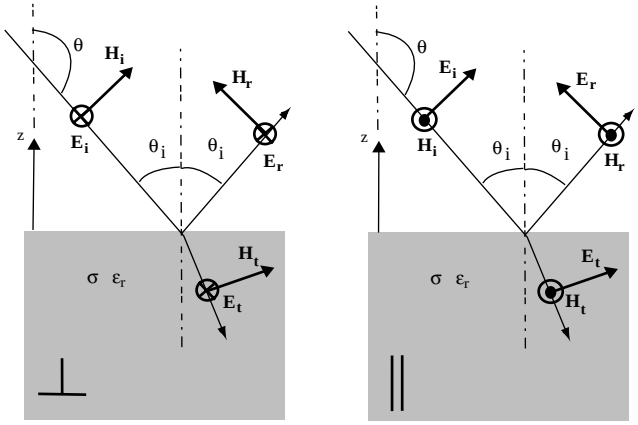

Figure 1: *Reflection and refraction at an interface between free space and a homogeneous half space. Left: Polarization perpendicular to the plane of incidence. Right: Polarization parallel to the plane of incidence.*

where

$$n = \sqrt{\epsilon_r - j\frac{\sigma}{\epsilon_0\omega}} \quad (5)$$

is the index of refraction of the lower half-space, θ_i is the incidence angle and a non-magnetic material is assumed. Note that for a lossy material the wave is an inhomogenous plane wave and the complex component $\mathbf{E}_t$, for parallel incidence in Fig. 1, has no real direction. In this case $T_{\parallel}$ may be interpreted as the relation between $(Z_0/n)H_t$ and $Z_0 H_i$, since the magnetic fields in both media are parallel (perpedicular to the plane of incidence). This will be used in section 3.2 when discussing the numerical equivalence to $T_{\parallel}$.

Using the analytical expressions (1) – (4) in FDTD gives spurious fields at the Huygens' surface because the FDTD-algorithm is not consistent with the analytical expressions. Below we will derive the Fresnel coefficients that are consistent with the FDTD-algorithm and we will show that the accuracy can be increased significantly in scattering simulations of weak scatterers.

3 Modified Fresnel coefficients

To derive Fresnel coefficients consistent with FDTD, the boundary value problem at the interface is solved by inserting FDTD consistent, instead of analytical, plane waves into the FDTD update equations.

The derivations below are divided into the two usual cases; the incident electric field transverse to the plane of

incidence (TE or $\perp$) and the incident electric field parallel to the plane of incidence (TM or $\parallel$). A monochromatic plane wave of amplitude U_0 will propagate in the FDTD grid according to

$$U|_{i,j,k}^n = U_0 e^{j\omega n\Delta t - j\tilde{\mathbf{k}}\cdot\mathbf{r}} \tag{6}$$

where $U|_{i,j,k}^n$ is an electric or magnetic field component at time step n at position (i,j,k) in the FDTD grid, $\tilde{\mathbf{k}} = \tilde{k}_x\hat{x} + \tilde{k}_y\hat{y} + \tilde{k}_z\hat{z}$ is the numerical wave vector and $\mathbf{r} = i\Delta x\hat{x} + j\Delta y\hat{y} + k\Delta z\hat{z}$.

The following parameters are useful for the derivations. They appear naturally when substituting the plane wave expressions into the temporal and spatial finite differences of FDTD, using a time-average for the conduction current term;

$$\widetilde{K}_x = \frac{2}{\Delta x}\sin\left(\frac{\tilde{k}_x\Delta x}{2}\right) \tag{7a}$$

$$\widetilde{K}_y = \frac{2}{\Delta y}\sin\left(\frac{\tilde{k}_y\Delta y}{2}\right) \tag{7b}$$

$$\widetilde{K}_z = \frac{2}{\Delta z}\sin\left(\frac{\tilde{k}_z\Delta z}{2}\right) \tag{7c}$$

$$\widetilde{K}_{tz} = \frac{2}{\Delta z}\sin\left(\frac{\tilde{k}_{tz}\Delta z}{2}\right) \tag{7d}$$

$$\tilde{\omega} = \frac{2}{\Delta t}\sin\left(\frac{\omega\Delta t}{2}\right) \tag{7e}$$

$$\tilde{\sigma} = \sigma\cos\left(\frac{\omega\Delta t}{2}\right) \tag{7f}$$

where $\tilde{k}_{tz}$ is the z-component of the numerical wave vector in the ground, which is complex if the ground is lossy ($\sigma \neq 0$). Using (7) the FDTD dispersion relation in free space is then simply written as

$$\frac{\tilde{\omega}^2}{c_0^2} = \widetilde{K}_0^2 = \widetilde{K}_x^2 + \widetilde{K}_y^2 + \widetilde{K}_z^2 \tag{8}$$

and in a homogeneous lossy ground as

$$\epsilon_r\frac{\tilde{\omega}^2}{c_0^2} - j\tilde{\sigma}\mu_0\tilde{\omega} = \tilde{n}^2\widetilde{K}_0^2 = \widetilde{K}_x^2 + \widetilde{K}_y^2 + \widetilde{K}_{tz}^2 \tag{9}$$

where $\tilde{n}$ is the FDTD index of refraction

$$\tilde{n}^2 = \epsilon_r - j\frac{\tilde{\sigma}}{\epsilon_0\tilde{\omega}}. \tag{10}$$

The incident wave vector can be written as

$$\begin{aligned}\tilde{k}_x &= \tilde{k}_0\cos\phi\sin\theta \\ \tilde{k}_y &= \tilde{k}_0\sin\phi\sin\theta \\ \tilde{k}_z &= \tilde{k}_0\cos\theta.\end{aligned} \tag{11}$$

Due to (7), the direction of $\widetilde{\mathbf{K}} = \widetilde{K}_x\hat{x} + \widetilde{K}_y\hat{y} + \widetilde{K}_z\hat{z}$ will generally not coincide with $\tilde{\mathbf{k}}$ except at certain angles. However, the difference is negligible, see Appendix A. We will therefore use

$$\begin{aligned}\widetilde{K}_x &= \widetilde{K}_0\cos\phi\sin\theta \\ \widetilde{K}_y &= \widetilde{K}_0\sin\phi\sin\theta \\ \widetilde{K}_z &= \widetilde{K}_0\cos\theta.\end{aligned} \tag{12}$$

which will actually make (11) an approximation. Using (9) and (12) yields

$$\widetilde{K}_{tz} = -\widetilde{K}_0\sqrt{\tilde{n}^2 - \sin^2\theta} \tag{13}$$

where we have chosen the minus sign since it is assumed in the derivation below that the refracted waves will propagate in the negative z-direction.

Consider the situation in Fig. 1. A plane wave is incident on a lossy homogeneous half-space at $z < 0$. The plane of incidence can be at an arbitrary angle ϕ with respect to the horizontal x-axis, i.e. we do not restrict the orientation of the incident plane to be parallel to the x- or y-axes in the FDTD-lattice. Since it is common to express the Fresnel coefficients in terms of the incident angle θ_i, this angle will be used below instead of the θ-angle for the incident wave vector. Since $\theta_i = \pi - \theta$, $\sin\theta_i = \sin\theta$ and $\cos\theta_i = -\cos\theta$.

3.1 Polarization perpendicular to the plane of incidence (TE)

When deriving the Fresnel coefficients for the TE-case, it is only necessary to use the field components in the $X-Z$-plane shown in Fig. 2 (an analysis using field components in the $Y-Z$-plane yields the same results). The exact position of the interface between the upper and lower half-spaces – illustrated with a faded shading in Fig. 2 – is so far undetermined. The only assumptions are that the $H_x|_{i,j,k+1/2}$ and $E_y|_{i,j,k+1}$ components in Fig. 2 are in the upper half-space and that the others are in the lower half-space. This is indicated with the horizontal dashed line in Fig. 2.

We also need to define the different horizontal electric field components E_x and E_y for the incident, reflected and refracted waves. In the upper medium we have

$$E_x^i = -\sin\phi e^{j\omega t - j\bar{k}_x x - j\bar{k}_y y - j\bar{k}_z z} \tag{14a}$$

$$E_x^r = -\widetilde{\Gamma}_\perp\sin\phi e^{j\omega t - j\bar{k}_x x - j\bar{k}_y y + j\bar{k}_z z} \tag{14b}$$

$$E_y^i = \cos\phi e^{j\omega t - j\bar{k}_x x - j\bar{k}_y y - j\bar{k}_z z} \tag{15a}$$

$$E_y^r = \widetilde{\Gamma}_\perp\cos\phi e^{j\omega t - j\bar{k}_x x - j\bar{k}_y y + j\bar{k}_z z} \tag{15b}$$

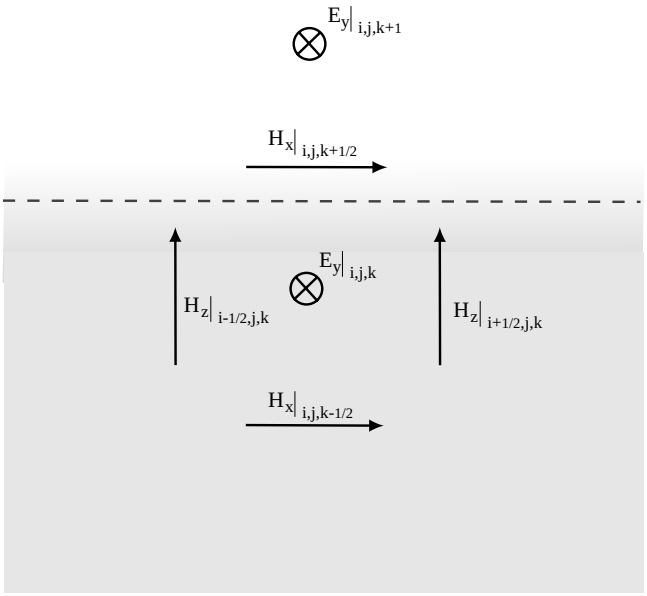

Figure 2: *FDTD field components used in the derivation of Fresnel coefficients for the TE-case. The dashed line does not represent the interface position, it just divides the field components into the two different half-spaces.*

and in the lower medium we have

$$E_x^t = -\widetilde{T}_\perp \sin\phi e^{j\omega t - j\tilde{k}_x x - j\tilde{k}_y y - j\tilde{k}_{tz} z} \quad (16)$$

$$E_y^t = \widetilde{T}_\perp \cos\phi e^{j\omega t - j\tilde{k}_x x - j\tilde{k}_y y - j\tilde{k}_{tz} z} \quad (17)$$

where $\widetilde{\Gamma}_\perp$ and $\widetilde{T}_\perp$ are the FDTD Fresnel coefficients yet to be determined. We also need the relationship between the electric and magnetic fields for each of the plane waves. Utilizing (7) we can rewrite the FDTD update equations for some of the magnetic fields as

$$\mu_0 j\tilde{\omega} H_x^i = -j\widetilde{K}_z E_y^i \quad (18a)$$

$$\mu_0 j\tilde{\omega} H_x^r = j\widetilde{K}_z E_y^r \quad (18b)$$

$$\mu_0 j\tilde{\omega} H_x^t = -j\widetilde{K}_{tz} E_y^t \quad (18c)$$

$$\mu_0 j\tilde{\omega} H_z^t = j\widetilde{K}_x E_y^t - j\widetilde{K}_y E_x^t. \quad (18d)$$

By inserting the plane wave expressions (14) – (17) into the FDTD update equations for $E_y|_{i,j,k}$ and $H_x|_{i,j,k+1/2}$, see Fig. 2, we are able to determine the unknown coefficients $\widetilde{\Gamma}_\perp$ and $\widetilde{T}_\perp$. We choose the phase reference point at the position of $E_y|_{i,j,k}$ in the middle of Fig. 2. Note that all components in Fig. 2 have the same y–coordinate ($y = 0$).

The update equation for $E_y|_{i,j,k}$ within the ground is

$$\epsilon_r\epsilon_0 \left(\frac{E_y|_{i,j,k}^{n+1/2} - E_y|_{i,j,k}^{n-1/2}}{\Delta t} \right) + \sigma \left(\frac{E_y|_{i,j,k}^{n+1/2} + E_y|_{i,j,k}^{n-1/2}}{2} \right) = \left(\frac{H_x|_{i,j,k+1/2}^n - H_x|_{i,j,k-1/2}^n}{\Delta z} \right) - \left(\frac{H_z|_{i+1/2,j,k}^n - H_z|_{i-1/2,j,k}^n}{\Delta x} \right). \quad (19)$$

Inserting the plane wave expression (17) for E_y into (19) the left hand side (LHS) of (19) becomes

$$\text{LHS} = (\epsilon_r\epsilon_0 j\tilde{\omega} + \tilde{\sigma})\widetilde{T}_\perp \cos\phi. \quad (20)$$

The magnetic field component $H_x|_{i,j,k+1/2}$ on the right hand side of (19) is in the free space region and therefore consists of an incident and a reflected part. Using (15), (18a) and (18b) we get

$$H_x|_{i,j,k+1/2} = -\left(e^{-j\frac{\tilde{k}_z\Delta z}{2}} - \widetilde{\Gamma}_\perp e^{j\frac{\tilde{k}_z\Delta z}{2}} \right) \frac{\widetilde{K}_z}{\mu_0\tilde{\omega}} \cos\phi \quad (21)$$

The other H_x component in (19) is in the lower half-space, using (17) and (18c) yield

$$H_x|_{i,j,k-1/2} = -\widetilde{T}_\perp e^{j\frac{\tilde{k}_{tz}\Delta z}{2}} \frac{\widetilde{K}_{tz}}{\mu_0\tilde{\omega}} \cos\phi. \quad (22)$$

The H_z–components are in the lower medium. Using (16), (17) and (18d), the spatial difference of H_z in (19) can then be written as

$$\frac{H_z|_{i+1/2,j,k} - H_z|_{i-1/2,j,k}}{\Delta x} = -j\widetilde{T}_\perp \frac{\widetilde{K}_x}{\mu_0\tilde{\omega}} (\widetilde{K}_x \cos\phi + \widetilde{K}_y \sin\phi) = -j\widetilde{T}_\perp \frac{\widetilde{K}_0^2 \sin^2\theta_i}{\mu_0\tilde{\omega}} \cos\phi \quad (23)$$

where we also have used (12). Using (20), (21), (22) and (23) in (19) now yield

$$(\epsilon_r\epsilon_0\mu_0 j\tilde{\omega}^2 + \mu_0\tilde{\omega}\tilde{\sigma})\widetilde{T}_\perp = -\left(\frac{e^{-j\frac{\tilde{k}_z\Delta z}{2}} - \widetilde{\Gamma}_\perp e^{j\frac{\tilde{k}_z\Delta z}{2}}}{\Delta z} \right) \widetilde{K}_z + \frac{\widetilde{T}_\perp \widetilde{K}_{tz} e^{j\frac{\tilde{k}_{tz}\Delta z}{2}}}{\Delta z} + j\widetilde{T}_\perp \widetilde{K}_0^2 \sin^2\theta_i. \quad (24)$$

The other equation needed is the update equation for

$H_x|_{i,j,k+1/2}$ above the ground:

$$\mu_0 \left(\frac{H_x|_{i,j,k+1/2}^{n+1} - H_x|_{i,j,k+1/2}^{n}}{\Delta t} \right) = \left(\frac{E_y|_{i,j,k+1}^{n+1/2} - E_y|_{i,j,k}^{n+1/2}}{\Delta z} \right). \quad (25)$$

Inserting plane wave expression for the H_x- and E_y- fields using (15), (17), (18a) and (18b) yields

$$-j\widetilde{K}_z \left(e^{-j\frac{\tilde{k}_z \Delta z}{2}} - \widetilde{\Gamma}_\perp e^{j\frac{\tilde{k}_z \Delta z}{2}} \right) = \left(\frac{e^{-j\bar{k}_z \Delta z} + \widetilde{\Gamma}_\perp e^{j\bar{k}_z \Delta z}}{\Delta z} \right) - \frac{\widetilde{T}_\perp}{\Delta z} \quad (26)$$

Solving the equation system (24) and (26) with respect to the two unknowns $\widetilde{\Gamma}_\perp$ and $\widetilde{T}_\perp$ yields

$$\widetilde{\Gamma}_\perp = \frac{\alpha \cos\theta_i - \beta\sqrt{\tilde{n}^2 - \sin^2\theta_i}}{\alpha^* \cos\theta_i + \beta\sqrt{\tilde{n}^2 - \sin^2\theta_i}} \quad (27)$$

$$\widetilde{T}_\perp = \frac{(\alpha + \alpha^*)\cos\theta_i}{\alpha^* \cos\theta_i + \beta\sqrt{\tilde{n}^2 - \sin^2\theta_i}} \quad (28)$$

where we have used (7c), (7d), (12) and (13). The coefficients α and β are factors corresponding to propagation across a half cell in the z–direction in the upper and lower medium respectively

$$\alpha = e^{-j\frac{\tilde{k}_z \Delta z}{2}} = e^{j\frac{\tilde{k}_0 \cos\theta_i \Delta z}{2}} \quad (29)$$

$$\beta = e^{-j\frac{\tilde{k}_{tz} \Delta z}{2}} = e^{j\frac{\tilde{k}_0 \sqrt{\tilde{n}^2 - \sin^2\theta_i} \Delta z}{2}}. \quad (30)$$

Note that the only ϕ–dependence of (27) and (28) are through the FDTD dispersion relation and the numerical wavenumber in (29) and (30).

As expected, (27) and (28) reduces to the analytical equations (2) and (4) as $\Delta x, \Delta y, \Delta z \to 0$. Also, note that when $|\tilde{n}| \to \infty$, as for a perfect conductor, $\widetilde{\Gamma}_\perp \to -1$, $\widetilde{T}_\perp \to 0$, i.e. the reflection occurs at the layer of electric field components at $z = 0$, while for $\tilde{n} = 1$ (when $\alpha = \beta$) $\widetilde{\Gamma}_\perp = 0, \quad \widetilde{T}_\perp = 1$.

If $\tilde{k}_0|\tilde{n}|\Delta z \ll 1$, $\widetilde{\Gamma}_\perp \approx \alpha^2 \Gamma_\perp$ and $\widetilde{T}_\perp \approx \alpha/\beta T_\perp$, which are equal to the analytical coefficients with the interface at $z = \Delta z/2$, as shown in Appendix B.

3.2 Polarization parallel to the plane of incidence (TM)

The coefficients for the TM-case can be found in a similar manner. Consider the components in the $X - Z$ -plane in Fig. 3. In this case only the H_z–components are zero. As in the TE-case we only need to consider the field components at $y = 0$. In the upper medium we have

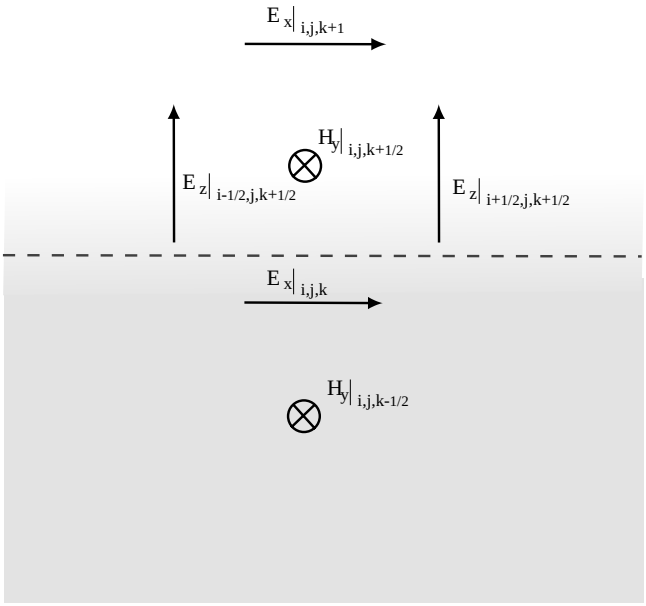

Figure 3: *FDTD field components used in the derivation of Fresnel coefficients for the TM-case. The dashed line does not represent the interface position, it just divides the field components into the two different half-spaces.*

$$E_x^i = \cos\theta_i \cos\phi e^{j\omega t - j\bar{k}_x x - j\bar{k}_y y - j\bar{k}_z z} \quad (31a)$$

$$E_x^r = -\widetilde{\Gamma}_\parallel \cos\theta_i \cos\phi e^{j\omega t - j\bar{k}_x x - j\bar{k}_y y + j\bar{k}_z z} \quad (31b)$$

$$E_y^i = \cos\theta_i \sin\phi e^{j\omega t - j\bar{k}_x x - j\bar{k}_y y - j\bar{k}_z z} \quad (32a)$$

$$E_y^r = -\widetilde{\Gamma}_\parallel \cos\theta_i \sin\phi e^{j\omega t - j\bar{k}_x x - j\bar{k}_y y + j\bar{k}_z z} \quad (32b)$$

$$E_z^i = \sin\theta_i \, e^{j\omega t - j\bar{k}_x x - j\bar{k}_y y - j\bar{k}_z z} \quad (33a)$$

$$E_z^r = \widetilde{\Gamma}_\parallel \sin\theta_i e^{j\omega t - j\bar{k}_x x - j\bar{k}_y y + j\bar{k}_z z} \quad (33b)$$

and in the lower medium we have

$$E_x^t = \widetilde{T}_{\parallel h} \cos\phi e^{j\omega t - j\bar{k}_x x - j\bar{k}_y y - j\bar{k}_{tz} z} \quad (34)$$

$$E_y^t = \widetilde{T}_{\parallel h} \sin\phi e^{j\omega t - j\bar{k}_x x - j\bar{k}_y y - j\bar{k}_{tz} z} \quad (35)$$

$$E_z^t = \widetilde{T}_{\parallel v} e^{j\omega t - j\bar{k}_x x - j\bar{k}_y y - j\bar{k}_{tz} z} \quad (36)$$

where $\widetilde{\Gamma}_\parallel$ is the reflection coefficient and $\widetilde{T}_{\parallel h}$ and $\widetilde{T}_{\parallel v}$ are horizontal and vertical refraction coefficients, respectively.

We also need relationships between E_x and H_y for the plane waves in both media analogous to (18):

$$j\tilde{\omega}\epsilon_0 E_x^i = j\widetilde{K}_z H_y^i \quad (37a)$$

$$j\tilde{\omega}\epsilon_0 E_x^r = -j\widetilde{K}_z H_y^r \quad (37b)$$

$$(j\tilde{\omega}\epsilon_0\epsilon_r + \tilde{\sigma})E_x^t = j\widetilde{K}_{tz} H_y^t \quad (37c)$$

The update equation for $H_y|_{i,j,k+1/2}$ in Fig. 3 is

$$-\mu_0\left(\frac{H_y|_{i,j,k+1/2}^{n+1} - H_y|_{i,j,k+1/2}^{n}}{\Delta t}\right) = \left(\frac{E_x|_{i,j,k+1}^{n+1/2} - E_x|_{i,j,k}^{n+1/2}}{\Delta z}\right) - \left(\frac{E_z|_{i+1/2,j,k+1/2}^{n+1/2} - E_z|_{i-1/2,j,k+1/2}^{n+1/2}}{\Delta x}\right) \quad (38)$$

We now define the phase reference point at the position of $E_x|_{i,j,k}$ (i.e. the same z-level as for TE–polarization), the only component in (38) that is in the lower medium, see Fig. 3. Inserting the plane wave expressions (31) – (36) into (38) and using (37) gives

$$-j\tilde{\omega}\mu_0\left(\frac{\tilde{\omega}\epsilon_0}{\widetilde{K}_z}e^{-j\frac{\tilde{k}_z\Delta z}{2}} + \frac{\tilde{\omega}\epsilon_0}{\widetilde{K}_z}\widetilde{\Gamma}_{\parallel}e^{j\frac{\tilde{k}_z\Delta z}{2}}\right)\cos\theta_i\cos\phi = \left(\frac{e^{-j\bar{k}_z\Delta z} - \widetilde{\Gamma}_{\parallel}e^{j\bar{k}_z\Delta z}}{\Delta z}\right)\cos\theta_i\cos\phi - \frac{\widetilde{T}_{\parallel h}\cos\phi}{\Delta z} + j\widetilde{K}_x\sin\theta_i\left(e^{-j\frac{\tilde{k}_z\Delta z}{2}} + \widetilde{\Gamma}_{\parallel}e^{j\frac{\tilde{k}_z\Delta z}{2}}\right) \quad (39)$$

The other update equation needed is for $E_x|_{i,j,k}$ in the lower medium.

$$\epsilon_r\epsilon_0\left(\frac{E_x|_{i,j,k}^{n+1/2} - E_x|_{i,j,k}^{n-1/2}}{\Delta t}\right) + \sigma\left(\frac{E_x|_{i,j,k}^{n+1/2} + E_x|_{i,j,k}^{n-1/2}}{2}\right) = -\left(\frac{H_y|_{i,j,k+1/2}^{n} - H_y|_{i,j,k-1/2}^{n}}{\Delta z}\right) \quad (40)$$

Inserting the plane wave expression (31) – (36) into (40) and using (37) gives

$$(\epsilon_r\epsilon_0 j\tilde{\omega} + \tilde{\sigma})\widetilde{T}_{\parallel h}\cos\phi = -\frac{\tilde{\omega}\epsilon_0}{\widetilde{K}_z\Delta z}e^{-j\frac{\tilde{k}_z\Delta z}{2}}\cos\theta_i\cos\phi - \frac{\tilde{\omega}\epsilon_0\widetilde{\Gamma}_{\parallel}}{\widetilde{K}_z\Delta z}e^{j\frac{\tilde{k}_z\Delta z}{2}}\cos\theta_i\cos\phi + \frac{(\epsilon_r\epsilon_0 j\tilde{\omega} + \tilde{\sigma})\widetilde{T}_{\parallel h}}{j\widetilde{K}_{tz}\Delta z}e^{j\frac{\tilde{k}_{tz}\Delta z}{2}}\cos\phi \quad (41)$$

Solving (39) and (41), using (12) and (13), with respect to the unknowns $\widetilde{\Gamma}_{\parallel}$ and $\widetilde{T}_{\parallel h}$ yields

$$\widetilde{\Gamma}_{\parallel} = \frac{\beta\tilde{n}^2\cos\theta_i - \alpha\sqrt{\tilde{n}^2 - \sin^2\theta_i}}{\beta\tilde{n}^2\cos\theta_i + \alpha^*\sqrt{\tilde{n}^2 - \sin^2\theta_i}} \quad (42)$$

$$\widetilde{T}_{\parallel h} = \frac{(\alpha + \alpha^*)\cos\theta_i\sqrt{\tilde{n}^2 - \sin^2\theta_i}}{\beta\tilde{n}^2\cos\theta_i + \alpha^*\sqrt{\tilde{n}^2 - \sin^2\theta_i}}. \quad (43)$$

Finally we need to determine $\widetilde{T}_{\parallel v}$. Using $\nabla\cdot\mathbf{E}^t = 0$ within the lower medium

$$\widetilde{\mathbf{K}}_t\cdot\mathbf{E}^t = \widetilde{T}_{\parallel h}\widetilde{K}_0\sin\theta_i - \widetilde{T}_{\parallel v}\widetilde{K}_0\sqrt{\tilde{n}^2 - \sin^2\theta_i} = 0 \quad (44)$$

which together with (43) yields

$$\widetilde{T}_{\parallel v} = \frac{(\alpha + \alpha^*)\sin\theta_i\cos\theta_i}{\beta\tilde{n}^2\cos\theta_i + \alpha^*\sqrt{\tilde{n}^2 - \sin^2\theta_i}}. \quad (45)$$

As in the analytical case we may define a total $\widetilde{T}_{\parallel}$ as the relation between $(Z_0/\tilde{n})\mathbf{H}^t$ and $Z_0\mathbf{H}^i$ (which are parallel), where $\mathbf{H} = (\widetilde{\mathbf{K}}\times\mathbf{E})/\tilde{\omega}\mu_0$. This yields

$$\widetilde{T}_{\parallel} = \frac{(\alpha + \alpha^*)\tilde{n}\cos\theta_i}{\beta\tilde{n}^2\cos\theta_i + \alpha^*\sqrt{\tilde{n}^2 - \sin^2\theta_i}}. \quad (46)$$

When $\Delta x, \Delta y, \Delta z \to 0$, the numerical Fresnel coefficients (42) and (46) converge to (1) and (3), respectively. Also, as expected, when $\theta_i = 0$, $\widetilde{T}_{\parallel v} = 0$, $\widetilde{T}_{\parallel h} = \widetilde{T}_{\perp}$ and $\widetilde{\Gamma}_{\parallel} = -\widetilde{\Gamma}_{\perp}$. The behaviour when $\tilde{k}_0|\tilde{n}|\Delta z \ll 1$ is similar to the TE–case although the phase variation is slightly more complicated, see Appendix B.

The derived Fresnel coefficients contain the FDTD index of refraction (10) consistent with the FDTD dispersion relation (9), and they are also modified with the factors α and β compared to the analytical ones. They are therefore referred to as "modified" Fresnel coefficients in the following text.

4 Reflection and refraction coefficients in a 1-D FDTD case

To demonstrate the accuracy of the model, a one dimensional FDTD simulation was performed where a Gaussian pulse was incident on a homogeneous medium with $\epsilon_r = 10$ and $\sigma = 0.01$ S/m. The reflected tangential H-field and the refracted tangential E-field adjacent to the interface were registered. The results were transformed into the frequency domain and the reflection and refraction coefficients were calculated. The results are shown in Fig. 4 together with the analytical Fresnel coefficients. The cell size was 0.01 m and the maximum frequency 2 GHz corresponds to 15 cells/wavelength in free space and only five cells/wavelength in the lossy medium.

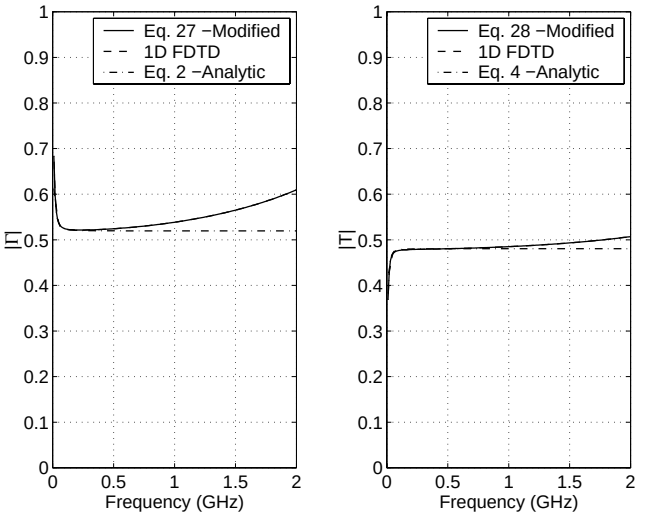

Figure 4: *Reflection and refraction at normal incidence on an interface between free space and a homogeneous half space. Left: Reflection coefficient. Right: Refraction coefficient. Note that the FDTD results and the predictions according to* (27) *and* (28) *are indistinguishable.*

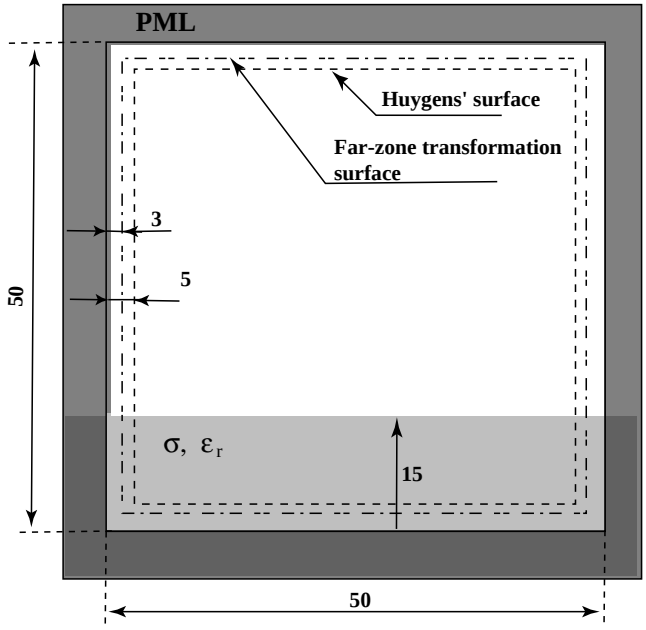

Figure 5: *X–Z slice of the computational volume at* $y = 20\Delta y$. *The Huygens' surface extends 10 cells below the ground. The far-zone transformation is performed in the scattered field region 2 cells outside the Huygens' surface.*

As seen from Fig. 4, the correspondence between the predicted FDTD results and the simulated FDTD results are excellent.

5 Plane wave incidence on an empty 3-D FDTD volume

The modified Fresnel coefficients (27), (28), (42), (43) and (45), were implemented in a 3-D FDTD code where they were used in the Huygens' routine as well as in the near- to far-zone transformation routine [12]. Scattering simulations were performed for an empty FDTD-volume in order to establish the lower limit of Radar Cross Section (RCS) simulations for a given problem size. Simulations were also performed using the analytical Fresnel coefficients as a reference case. The plane of reflection for the analytical coefficients (1)–(4) was positioned at the layer of tangetial magnetic field components, $\Delta z/2$ above the phase reference point used in the derivations of the modiefied Fresnel coefficients. This gives the most accurate results for analytical Fresnel coefficients. A motivation for this can be found in Appendix B.

When calculating the Huygens' sources in the free-space region, the incident and reflected pulse propagations were dispersion compensated according to [14]. For the Huygens' sources within the ground, this dispersion compensation procedure was applied on the propagation occurring in the free space region before entering the lossy ground. The dispersion of the pulse due to propagation within the lossy ground was then taken into account, using the numerical wavenumbers when calculating the pulses in the frequency domain at each horizontal layer. The dispersion compensation was not used in the reference case since its effect is small compared to the adjustment of the Fresnel coefficients.

The pulse functions were pre-calculated and stored in arrays, field values were extracted using a table-look up procedure [18] and a third order Lagrange interpolation. A Gaussian derivative pulse was used for the incident plane wave. The pulse function was $E_{inc} = \tau\sqrt{2e}\exp(-\tau^2)$ V/m, where $\tau = 4/(\beta\Delta t)(t - 1.5\beta\Delta t)$ with $\beta = 80$. The computational volume consisted of $50 \times 40 \times 50$ cubic cells, see Fig. 5 ($\Delta x = \Delta y = \Delta z = 0.01$ m). The outer boundary was terminated by a 6-cell-thick PML [21]. The PML within the ground was treated in a similar way as in [22].

A Huygens' surface was positioned five cells from the outer boundary. The upper level of the lossy half-space was 15 cells from the lower PML-region, see Fig. 5. As before, the parameters for the ground were $\epsilon_r = 10$ and $\sigma = 0.01$ S/m ($\lambda = 15$ cells at 2 GHz in the free space region and only 5 cells within ground).

Three different incident angles were used in the simulations; $\theta_i = 0°$(normal incidence), $\theta_i = 45°$, $\phi = 0$

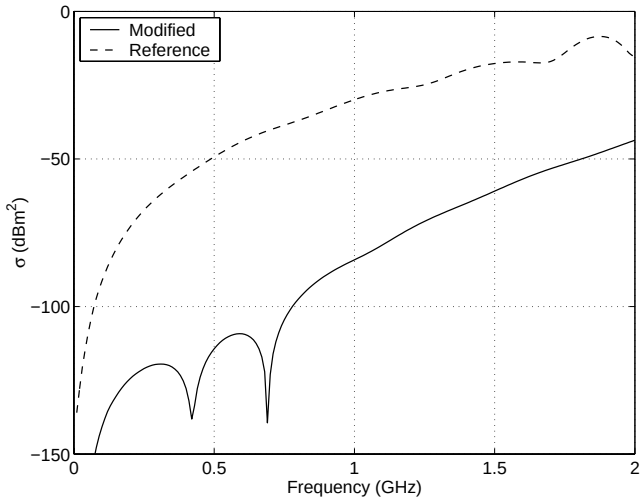

Figure 6: *Monostatic RCS of empty FDTD volume as function of frequency. Incidence angle* $\theta_i = 0°$.

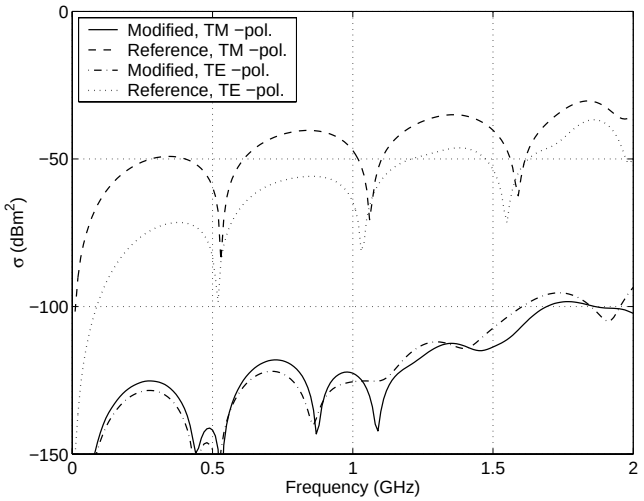

Figure 7: *Monostatic RCS of empty FDTD volume as function of frequency. Incidence angle* $\theta_i = 45°$, $\phi = 0°$. *Both TE- and TM- results are shown.*

and $\theta_i = 45°$, $\phi = 30°$. Both TE- and TM- polarizations were used in the $\theta_i = 45°$, $\phi = 0°$–case. In the other cases TM-polarization were used (both polarizations coincide for the $\theta_i = 0°$–case). The scattered field was determined using a time-domain near-zone to far-zone transformation applied three cells from the outer boundary [12]. Both monostatic and bistatic RCS results were calculated. The results using the modified Fresnel coefficients are labeled "Modified" in Figs. 6– 12. The corresponding results using the analytical expressions for the Fresnel coefficients (including phase corrections) are labeled "Reference".

The effects of using modified Fresnel coefficients on the far-zone scattered field are illustrated in Figs. 6–9 where the monostatic and bistatic RCS of an empty FDTD volume are shown for four cases of incident directions. The scattered field is calculated in the same polarization as the incident field. The volume enclosed by the Huygens' surface is $0.4 \times 0.3 \times 0.4$ m^3.

As seen from the figures, the RCS level of the empty volume has been reduced by $30 - 60$ dB using the modified Fresnel coefficients. The RCS level is higher for TM–polarization than for TE–polarization in the reference case, according to Figs. 7 and 8. The reason is that the reflection plane offset of $\Delta z/2$ is a better approximation for TE- than for TM-polarization according to Appendix B.

The use of modified Fresnel coefficients does not affect the computational time during the FDTD main loop since the incident pulse functions are pre-calculated and stored in tables. The time increase in using the modified Fresnel coefficients compared to the analytical ones has been measured to $\approx 5\%$ when calculating the frequency domain pulse spectra before the main loop. In the near- to far-zone transformation, the Fresnel coefficients are applied after the main loop according to [12] which consequently does not affect the computational time of the main loop either.

The demonstrated reduction of the RCS noise level is important when studying low level scattering, such as for buried objects. An example of this follows in section 6.

6 Scattering from a dipole

A resonant dipole buried 0.2 meters below the ground level was chosen as an example of a scattering object. The dipole length was 0.21 m and the radius 1 mm. The RCS of the dipole was calculated using the Method of Moment program NEC-3 and the FDTD method, both with analytical and modified Fresnel coefficients. A thin wire model according to [18] was used for the dipole which was oriented in the x-direction. The dipole was modeled using 20 cells, which corresponds to a true dipole length of 0.21 m since the staircasing effect in FDTD causes the electric dipole length to increase with a half cell-size at each end.

The computational volume, cell size, positions of Huygens' and near- to far-zone transformation surfaces and ground parameters were identical as in the previous section. The only difference was the position of the ground level, which was 35 cells from the lower PML-boundary, see Fig. 10. The dipole was positioned 0.205 m below the ground level in the NEC-3 simulation since the main reflection occurs at the level of tangential magnetic fields,

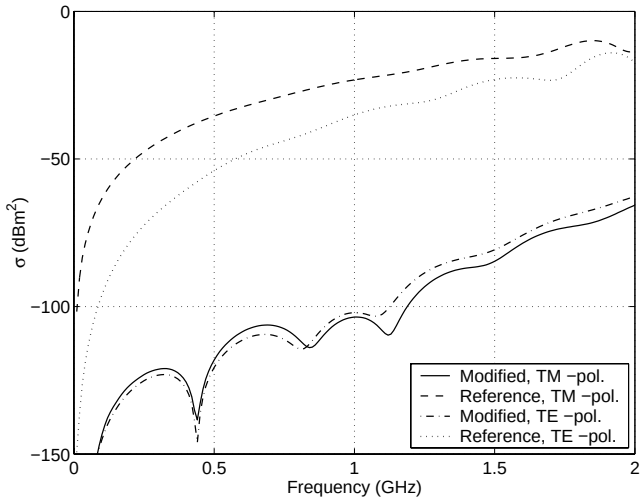

Figure 8: *Bistatic RCS of empty FDTD volume as function of frequency. Incidence angle* $\theta_i = 45°$, $\phi = 0°$. *Scattering in specular direction. Both TE- and TM- results are shown.*

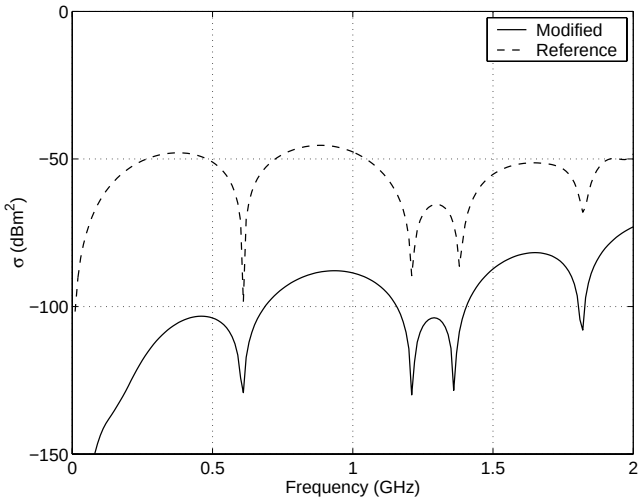

Figure 9: *Monostatic RCS of empty FDTD volume as function of frequency. Incidence angle* $\theta_i = 45°$, $\phi = 30°$. *TM-polarization.*

as discussed in Appendix B.

The plane wave was incident in the same plane as the dipole at $\theta_i = 45°$. The frequency band was restricted to be below 1 GHz using a slightly narrower pulse spectrum, compared to the empty volume simulations in section 5 ($\epsilon_r = 10$ and $\sigma = 0.01$ S/m yield approximately 10 cells/wavelength at 1 GHz in the ground). The incident field was applied using a modulated Gaussian pulse with $E_{inc} = \cos(2\pi f_0[t - 1.5\beta\Delta t])\exp(-\tau^2)$ V/m, where $\tau = 4/(\beta\Delta t)(t - 1.5\beta\Delta t)$ with $\beta = 320$ and $f_0 = 0.5$ GHz.

As a reference, the monostatic RCS was calculated *without* the dipole in FDTD using both the modified and analytical Fresnel coefficients in the Huygens routine.

The monostatic RCS of the dipole can be seen in Fig. 11. Both the modified and the analytical Fresnel coefficients have been used in the FDTD simulations. For comparison, the scattering result for an empty FDTD -volume *without* the dipole using the analytical Fresnel coefficients is also shown in the graph as a dashed-dotted line (the RCS-level of the empty FDTD-volume using the modified Fresnel coefficients are below -120 dBm^2 in this case). As before, results using analytical Fresnel coefficients are labeled "Reference". Obviously, the scattered field in the reference case without the dipole is of the same order as the scattered field from the dipole. Hence, the poor correspondence with the NEC-result in this case. There is a difference between the NEC- results and the FDTD-results using modified Fresnel coefficients which is due to the poor resolution in the ground (only 10 cells per wavelength at 1 GHz) and to the thin-wire model in FDTD. Also, since the modified Fresnel coefficients are different from the ones in NEC-3, the refracted fields reaching the dipole are slightly different in the two models. This has been verified in a simulation using twice as high resolution in FDTD, which showed better convergence between FDTD- and NEC- results.

It is often of interest to study the time-domain response of the electric fields for these type of scattering simulations. The scattered electric far-fields from the NEC-3 were therefore Fourier transformed into the time-domain after multiplication by the incident pulse spectrum used in the FDTD-simulations. The far-fields in FDTD were calculated in the time-domain using the method described in [12]. The phase reference point was set at the surface straight above the dipole, see point P in Fig. 10. To get a distance independent result, the voltage rE_θ was extracted from the simulations.

FDTD results without the dipole is shown in top of Fig. 12. using both the modified and analytical Fresnel coefficients. In the reference case, the signal appears slightly before $t = 0$ due to the disturbance at left intersection between the ground and the Huygens' surface in Fig. 10.

The time domain results with the dipole in place is shown in the bottom of Fig. 12 including the NEC-3 result. As seen from the graphs, the correspondence is very good except for the FDTD reference-case. After the disturbance from the Huygens' surface has vanished, the signals are nearly identical. If a larger region would be used, the error would increase as the side length of the Huygens' surface increases.

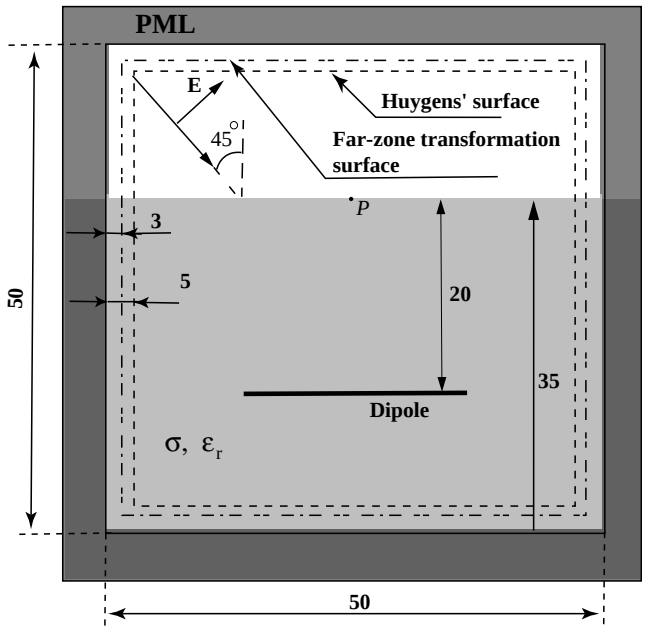

Figure 10: *X–Z slice of the computational volume at $y = 20\Delta y$ for the dipole case. The Huygens' surface extends 30 cells below the ground. The far-zone transformation is performed in the scattered field region 2 cells outside the Huygens' surface. The dipole is positioned 20 cells below the ground level (of tangential electric field components in FDTD)*

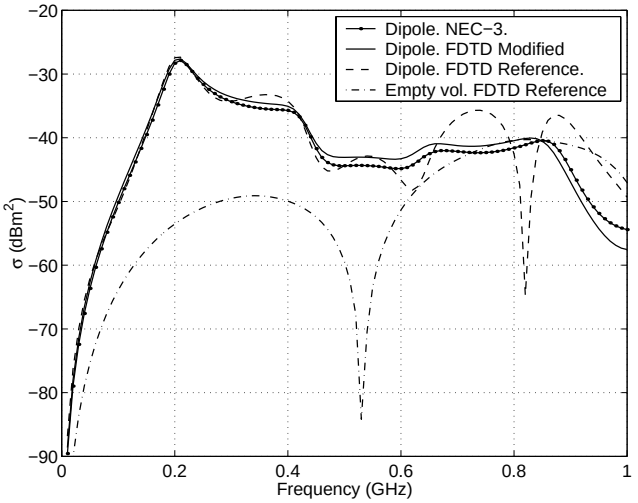

Figure 11: *Monostatic RCS of buried dipole 0.205 m below the ground level. Incidence angle $\theta_i = 45°$, $\phi = 0°$. TM- polarization.*

7 Conclusions

Fresnel coefficients for a homogeneous lossy dielectric half-space, consistent with the FDTD algorithm have been derived. The coefficients are valid for arbitrary incidence angles in a 3D FDTD simulation. Using these coefficients in the Huygens' routine reduce the errors significantly. The improvements achieved have been demonstrated for a scattering simulation of a buried dipole in a homogeneous lossy dielectric half-space. The modified Fresnel coefficients lowers the limits of RCS-levels possible to simulate with FDTD, where plane wave incidence on a homogeneous ground is considered.

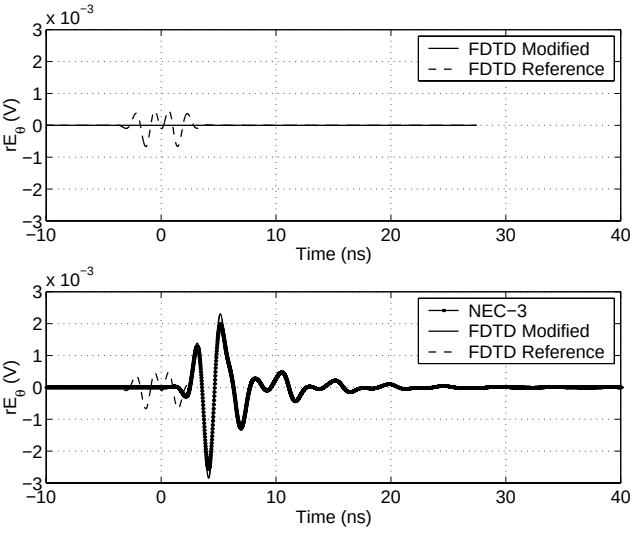

Figure 12: *Time response of the monostatic scattering from a buried dipole 0.205 m below the ground level (bottom) and without dipole (top). Incidence angle $\theta_i = 45°$, $\phi = 0°$. TM-polarization.*

Appendix A Incident angle approximation

The validity of the numerical incident angle approximation can be illustrated by taking the dot product between $\hat{\tilde{\mathbf{k}}} = \tilde{\mathbf{k}}/\tilde{k}_0$ and $\hat{\tilde{\mathbf{K}}} = \tilde{\mathbf{K}}/\tilde{K}_0$. Using the series expansion $\sin x \approx x - x^3/6 + O(x^5)$ in (7a)–(7c), the dot product can be written as

$$\begin{aligned}\hat{\tilde{\mathbf{k}}} \cdot \hat{\tilde{\mathbf{K}}} &= \frac{\tilde{\mathbf{k}} \cdot \tilde{\mathbf{K}}}{\tilde{k}_0 \tilde{K}_0} = \frac{\tilde{k}_x \tilde{K}_x + \tilde{k}_y \tilde{K}_y + \tilde{k}_z \tilde{K}_z}{\tilde{k}_0 \tilde{K}_0} = \\ &= \frac{\tilde{k}_x^2 - \frac{\bar{k}_x^4 \Delta x^2}{24} + \tilde{k}_y^2 - \frac{\bar{k}_y^4 \Delta y^2}{24} + \tilde{k}_z^2 - \frac{\bar{k}_z^4 \Delta z^2}{24}}{\tilde{k}_0 \sqrt{\tilde{K}_x^2 + \tilde{K}_y^2 + \tilde{K}_z^2}} \\ &+ O\left[(\tilde{k}_\nu \Delta\nu)^4\right], \nu = x, y, z.\end{aligned} \tag{A.1}$$

The square root can be expanded further and if we introduce the variable p, where

$$p^2 = s_x^4 \Delta x^2 + s_y^4 \Delta y^2 + s_z^4 \Delta z^2 \tag{A.2}$$

$$s_x = \cos\phi \sin\theta, \quad s_y = \sin\phi \sin\theta, \quad s_z = \cos\theta \tag{A.3}$$

we can rewrite (A.1) as

$$\begin{aligned}\hat{\tilde{\mathbf{k}}} \cdot \hat{\tilde{\mathbf{K}}} &= \frac{\tilde{k}_0^2 \left[\left(1 - \frac{\bar{k}_0^2 p^2}{24}\right) + O(\tilde{k}_0^4 p^4)\right]}{\tilde{k}_0^2 \sqrt{1 - \frac{\bar{k}_0^2 p^2}{12} + O(\tilde{k}_0^4 p^4)}} = \\ &= \frac{\left(1 - \frac{\bar{k}_0^2 p^2}{24}\right) + O(\tilde{k}_0^4 p^4)}{\left(1 - \frac{\bar{k}_0^2 p^2}{24}\right) + O(\tilde{k}_0^4 p^4)} = 1 + O(\tilde{k}_0^4 p^4).\end{aligned} \tag{A.4}$$

This result indicates that the angle approximation (12) is very accurate.

Appendix B Low frequency expansion of Fresnel coefficients

Consider the reflection coefficient $\widetilde{\Gamma}_\perp$. Moving an α^2 factor outside the expression (27) and expanding the remaining factors α and β up to first order we get

$$\begin{aligned}\widetilde{\Gamma}_\perp &= \alpha^2 \left[\frac{\cos\theta_i - \left(1 - \frac{j\bar{k}_0 \cos\theta_i \Delta z}{2} + \frac{j\bar{k}_0 \widetilde{N} \Delta z}{2}\right) \widetilde{N}}{\cos\theta_i + \left(1 + \frac{j\bar{k}_0 \cos\theta_i \Delta z}{2} + \frac{j\bar{k}_0 \widetilde{N} \Delta z}{2}\right) \widetilde{N}}\right] \\ &+ O\left[(\tilde{k}_0 \widetilde{N} \Delta z)^2\right]\end{aligned} \tag{B.1}$$

where we have introduced $\widetilde{N} = \sqrt{\tilde{n}^2 - \sin^2\theta_i}$ and used

$$\begin{aligned}\tilde{k}_{tz} &= -\tilde{k}_0 \widetilde{N} \\ \tilde{k}_z &= -\tilde{k}_0 \cos\theta_i.\end{aligned} \tag{B.2}$$

Rewriting (B.1) yields

$$\begin{aligned}\widetilde{\Gamma}_\perp &= \alpha^2 \left[\frac{\left(\cos\theta_i - \widetilde{N}\right)\left(1 + \frac{j\bar{k}_0 \widetilde{N} \Delta z}{2}\right)}{\left(\cos\theta_i + \widetilde{N}\right)\left(1 + \frac{j\bar{k}_0 \widetilde{N} \Delta z}{2}\right)}\right] + O\left[(\tilde{k}_0 \widetilde{N} \Delta z)^2\right] \\ &= \alpha^2 \Gamma_\perp + O\left[(\tilde{k}_0 \widetilde{N} \Delta z)^2\right].\end{aligned} \tag{B.3}$$

This indicates that for low frequencies –and not too high $|\tilde{n}|$– the modified reflection coefficient $\widetilde{\Gamma}_\perp$ converges into the analytical reflection coefficient times the phase factor α^2, corresponding to a shift in the reference point by $\Delta z/2$ in the z-direction. A similar analysis for $\widetilde{T}_\perp$ gives

$$\widetilde{T}_\perp = \frac{\alpha}{\beta} T_\perp + O\left[(\tilde{k}_0 \widetilde{N} \Delta z)^2\right] \tag{B.4}$$

which also corresponds to a shift of the reference point by $\Delta z/2$ (α) and an attenuation of the plane wave for that distance ($1/\beta$).

Analogous analysis for $\widetilde{\Gamma}_\parallel$ and $\widetilde{T}_\parallel$ gives slightly more complicated results. It can be shown that,

$$\widetilde{\Gamma}_\parallel = \alpha^{2+\gamma} \Gamma_\parallel + O\left[(\tilde{k}_0 \widetilde{N} \Delta z)^2\right] \tag{B.5}$$

and

$$\widetilde{T}_\parallel = \frac{\alpha^{1+\varepsilon_1}}{\beta^{1+\varepsilon_2}} T_\parallel + O\left[(\tilde{k}_0 \widetilde{N} \Delta z)^2\right] \tag{B.6}$$

where γ, ε_1 and ε_2 are proportional to θ_i^2 for small values of θ_i. These phase factors are thus not so well approximated by a simple shift of the reference plane as for perpendicular (TE) polarization.

References

[1] K. Demarest, R. Plumb, and Z. Huang, "FDTD modeling of scatterers in stratified media," *IEEE Trans. Antennas Propagat.*, vol. 43, no. 10, pp. 1164–1168, Oct. 1995.

[2] P. B. Wong, G. L. Tyler, J. E. Baron, E. M. Gurrola, and R. A. Simpson, "A three-wave FDTD approach to surface scattering with applications to remote sensing of geophysical surfaces," *IEEE Trans. Antennas Propagat.*, vol. 44, no. 4, pp. 504–513, 1996.

[3] K. Demarest, Z. Huang, and R. Plumb, "An FDTD near- to far-zone transformation for scatterers buried in stratified grounds," *IEEE Trans. Antennas Propagat.*, vol. 44, no. 8, pp. 1150–1157, 1996.

[4] T. Dogaru and L. Carin, "Time-domain sensing of targets buried under a rough air-ground interface," *IEEE Trans. Antennas Propagat.*, vol. 46, no. 3, pp. 360–372, 1998.

[5] T. Martin and L. Ulander, "Far-zone transformation in FDTD for VHF-band SAR-image simulations," in *ACES 98.*, Monterey, CA, March, 16–20 1998, vol. 1, pp. 79–86.

[6] F.L. Teixeira, W.C. Chew, M. Straka, M.L Oristaglio, and T. Wang, "Finite-difference time-domain simulation of ground penetrating radar on dispersive, inhomogenous, and conductive soils," *IEEE Trans. Geosci. Remote Sensing.*, vol. 36, no. 6, pp. 1928–1937, Nov. 1998.

[7] N. Geng, M.A. Ressler, and L. Carin, "Wide-band VHF scattering from a trihedral reflector situated above a lossy dispersive halfspace," *IEEE Trans. Geosci. Remote Sensing.*, vol. 37, no. 5, pp. 2609–2617, Sept. 1999.

[8] Z. Huang, K. R. Demarest, and R. G. Plumb, "An FDTD/MoM hybrid technique for modeling complex antennas in the presence of heterogeneous grounds," *IEEE Transactions on Geoscience and Remote Sensing*, vol. 37, no. 6, pp. 2692–2698, Nov. 1999.

[9] H. Israelsson, L. H. M. Ulander, T. Martin, and J. I. H. Askne, "A coherent scattering model to determine forest backscattering in the VHF-band," *IEEE Transactions on Geoscience and Remote Sensing*, vol. 38, no. 1, pp. 238–248, Jan. 2000.

[10] L. Gürel and U. Oğuz, "Three-dimensional FDTD modeling of a ground-penetrating radar," *IEEE Transactions on Geoscience and Remote Sensing*, vol. 38, no. 4, pp. 1513–1521, July 2000.

[11] N. Geng, A. Sullivan, and L. Carin, "Multilevel fast-multipole algorithm for scattering from conducting targets above or embedded in a lossy half space," *IEEE Trans. Geosci. Remote Sensing.*, vol. 38, no. 4, pp. 1561–1573, July 2000.

[12] T. Martin and L. Pettersson, "FDTD time domain near- to far-zone transformation above a lossy dielectric half-space," *Appl. Comput. Electromagn. Soc. J.*, vol. 16, no. 1, pp. 45–52, Mar. 2001.

[13] D. E. Merewether, R. Fisher, and F. W. Smith, "On implementing a numeric Huygen's source scheme in a finite difference program to illuminate scattering bodies," *IEEE Trans. Nucl. Sci.*, vol. 27, no. 6, pp. 1829–1833, Dec. 1980.

[14] T. Martin and L. Pettersson, "Dispersion compensation for Huygens' sources and far-zone transformation in FDTD," *IEEE Trans. Antennas Propagat.*, vol. 48, no. 4, pp. 494–501, Apr. 2000.

[15] T. Hirono, Y. Shibata, W. W. Lui, S. Seki, and Y. Yoshikuni, "The second-order condition for the dielectric interface orthogonal to the Yee-lattice axis in the FDTD scheme," *IEEE Microwave Guided Wave Lett.*, vol. 10, no. 9, pp. 359–361, Sept. 2000.

[16] A. Akyurtlu, D. H. Werner, V. Veremey, D. J. Steich, and K. Aydin, "Staircasing errors in FDTD at an air-dielectric interface," *IEEE Microwave Guided Wave Lett.*, vol. 9, no. 11, pp. 444–446, Nov. 1999.

[17] J. Fang and Z. Wu, "Closed-form expression of numerical reflection coefficient at PML interfaces and optimization of PML performance," *IEEE Microwave Guided Wave Lett.*, vol. 6, no. 9, pp. 332–334, Sept. 1996.

[18] A. Taflove, *Computational Electrodynamics: The Finite-Difference Time-Domain Method*, Artech House, Boston, MA, 1995.

[19] U. Oğuz, L. Gürel, and O. Arikan, "An efficient and accurate technique for the incident-wave excitation in the FDTD method," *IEEE Trans. Microwave Theory Tech.*, vol. 46, no. 6, pp. 869–882, June 1998.

[20] J. D. Jackson, *Classical Electrodynamics*, Wiley, New York, third edition, 1998.

[21] J.-P. Berenger, "A perfectly matched layer for the absorption of electromagnetic waves," *J. Comput. Phys.*, vol. 114, no. 1, pp. 185–200, 1994.

[22] J. Fang and Z. Wu, "Generalized perfectly matched layer for the absorption of propagating and evanescent waves in lossless and lossy media," *IEEE Trans. Microwave Theory Tech.*, vol. 44, no. 12, pp. 2216–2222, Dec. 1996.